Wetting of Macromolecules: From Linear Chain to Soft Colloid-Like Behavior

ARTICLE *in* MACROMOLECULES · JANUARY 2014

Impact Factor: 5.8 · DOI: 10.1021/ma4024119

5 AUTHORS, INCLUDING:

Emmanouil Glynos
University of Michigan
42 PUBLICATIONS **335** CITATIONS
SEE PROFILE

Alexandros Chremos
National Institute of Standards and Technology
30 PUBLICATIONS **270** CITATIONS
SEE PROFILE

Georgios Sakellariou
National and Kapodistrian University of Athens
58 PUBLICATIONS **605** CITATIONS
SEE PROFILE

Peter F Green
University of Michigan
93 PUBLICATIONS **1,586** CITATIONS
SEE PROFILE

Macromolecules

Article

pubs.acs.org/Macromolecules

Wetting of Macromolecules: From Linear Chain to Soft Colloid-Like Behavior

Emmanouil Glynos,[†] Alexandros Chremos,[‡] Bradley Frieberg,[§] Georgios Sakellariou,[∥] and Peter F. Green*[,†,§,⊥]

[†]Department of Materials Science and Engineering, [§]Macromolecular Science and Engineering, and [⊥]Biointerfaces Institute, University of Michigan, Ann Arbor, Michigan 48109, United States

[‡]Department of Chemical Engineering, Centre for Process Systems Engineering, Imperial College of London, South Kensington Campus, London SW7 2AZ, U.K.

[∥]Department of Chemistry, University of Athens, Panepistimiopolis, Zografou, 15771, Athens, Greece

ABSTRACT: The ability to control the wetting properties of a polymeric liquid on a given surface is important for several emerging technological applications including protective coatings, lubricants and sensors. Here we show that star-shaped polystyrene (PS) molecules exhibit notably different wetting properties than their linear analogues of the same chemical structure and their wetting properties can be controlled through changes of their functionality f (number of arms per molecule). Unlike linear chains, the wetting of star-shaped macromolecules is determined by the competition between entropic forces. Wetting is enhanced due to reductions in the loss of entropy upon adsorption of the stars with increasing f; soft colloidal-like entropic repulsion effects suppress the ability of the stars to exhibit a high degree of surface adsorption and to efficiently pack, for sufficiently large values of f. This phenomenon is manifested in the existence of a minimum in the macroscopic contact angle and other related microscopic parameters embodied in the effective interface potential as a function of f.

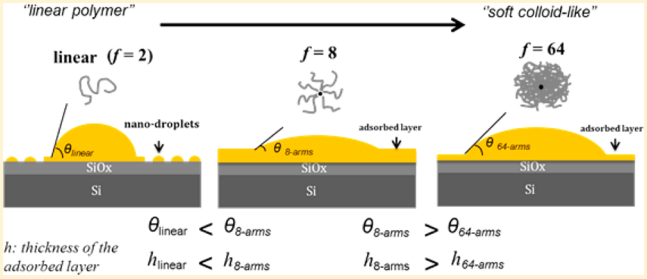

INTRODUCTION

The wetting of a nonvolatile liquid droplet on a surface is determined by a combination of short- and long-range intermolecular forces and the macroscopic contact angle, θ_∞, in the three-phase region is well described by Young's equation $\gamma \cos \theta_\infty = \gamma_{SV} - \gamma_{SL}$, where γ is the surface tension of the liquid, γ_{SV} is the bare surface energy of the substrate, and γ_{SL} is the interfacial tension between the liquid and the substrate.[1−5] The shape of the droplet in the vicinity of the line of contact is deformed due to effects of the long- and short-range intermolecular forces. Molecules in contact with the substrate experience a short-range interaction wherein the liquid/vapor interface is locally deformed. At length scales larger than $\alpha = (-A/(6\pi\gamma))^{1/2}$, where A is the Hamaker constant, deformation is due to the action of algebraically decaying long-ranged van der Waals forces. The shape of a droplet, away from the line of contact, is well approximated by a spherical cap when its radius is smaller than the capillary length $k = (\gamma/\rho g)^{1/2}$, where ρ is the mass density of the liquid and g the gravitational force.

One effective strategy to create droplets of different sizes on a nonwetting substrate is to prepare films of different thicknesses, h, on substrates and induce them to dewet. The initial film thickness determines the size of the droplets, so droplets of nanoscale dimensions are readily prepared. The thermodynamic behavior of the liquid film/substrate system in an environment may be formally understood in terms of an effective interface potential, $\phi(h)$, the excess free energy of interaction per unit area, that embodies the influence of the long- and short- range intermolecular forces.[6−9] Antagonistic long-range van der Waals interactions between the film/substrate and the film/air (or external vapor) interfaces are responsible for the dewetting of sufficiently thin films on substrates. In the case of polystyrene (PS) on silicon oxide substrates (SiO_x), antagonistic long- and attractive short-ranged interactions give rise to a minimum in $\phi(h)$, which suggests that at macroscopic droplets should reside on an adsorbed layer of thickness h^*.[9−14] The PS films dewet to form spinodal patterns or nucleation and growth patterns, dictated by the local curvature of $\phi(h)$. For linear chain PS thin films on SiO_x, it is observed after dewetting that macroscopic droplets are surrounded by a dense collection of significantly smaller droplets with diameters of several tens of nanometers.[13,14] These so-called nanodroplets are believed to be remnants of the thin adsorbed layer of thickness h^* that broke-up, due to chain conformational entropic effects when the liquid film is cooled from the melt and solidifies, forming a glass.[15]

In recent years different strategies, including grafting polymer chains onto substrates to alter the film/substrate interfacial

Received: November 25, 2013
Revised: January 9, 2014
Published: January 31, 2014

   dx.doi.org/10.1021/ma4024119 | *Macromolecules* 2014, 47, 1137−1143

interactions, or varying the thickness of coatings on substrates, have been employed to control the influence of the long- and short-range intermolecular interactions on the equilibrium structure of the polymers.[9,11,16,17] Dewetting experiments of 4-arm star-shaped poly(4vinylbenzyl chloride) (pVBC) films onto silanized Si wafers by Xu et al. showed that the receding contact angle, as measured by the profile of the rim during dewetting, of the 4-arm star-shaped polymer is smaller than that of linear PS on the same substrate.[18] They interpreted they data in terms of a stronger affinity of the substrate with the 4-arm star-shaped pVBC compared to the linear PS. Recently we showed that upon changing the architecture of the macromolecule from a linear chain to a star-shaped macromolecule, with a functionality f (number of arms) of 8, the macroscopic contact angle, θ_∞, decreased by more than an order of magnitude.[19] Moreover, the macroscopic droplets of this 8-arm star-shaped polymer resided on a layer of polymer of thickness $h^* = 7.5$ nm. This behavior was understood in terms of the enhanced adsorption of star-shaped polymers on surfaces, stemming from a decreased entropic penalty upon adsorption onto a substrate with increasing f. This behavior can be thought of as an increased entropic attraction of the star-shaped polymer, compared to the linear chains of the same chemical composition and degree of polymerization, on the same substrate.[20−23]

The more general and indeed interesting questions regarding the wetting of star-shaped polymers are related to what determines their wetting behavior when f becomes quite large and the macromolecules would potentially exhibit a more soft colloidal-like character. Through a combination of experiments and molecular dynamics simulations we show that the wetting behavior of star-shaped molecules is determined by a competition between their entropically enhanced adsorption onto surfaces with increasing f, and an opposing soft steric entropic repulsion that limits their ability to adsorb and closely "pack" onto the substrate. These competing entropic effects result in the existence of a minimum in the macroscopic contact angle and other associated microscopic parameters embodied in the effective interface potential as a function of f.

EXPERIMENTAL SECTION

1. Materials. A series of star-shaped molecules, with f ranging from 3 to 64 arms were synthesized and examined in this study. The star-shaped polymers with $f \leq 8$ were purchased from Polymer Sources (Polymer Source Inc. Canada). Star-shaped polymers with $f = 16$, 32, and 64 were synthesized by means of anionic polymerization using high vacuum techniques.[24−26] The materials used in this study are described in Table 1.

2. Thin Film Preparation and Atomic Force Microscopy (AFM) Measurements. The polymer films were prepared by spin-coating solutions onto cleaned oxidized silicon substrates, SiO_x (Wafer World Inc.). The oxidized silicon wafers were cleaned using the same procedure as that used in our previous study.[19] The thickness of the oxide layer was determined using spectroscopic ellipsometry to be $d_{ox} \approx 1.4$ nm. Prior to spin-casting, the solutions were filtered through 0.2 μm Teflon Millipore filters. The films were annealed at 160 °C in vacuum until the dewetting and the formation of macroscopic droplets formation was completed. The dewetted structures were probed using tapping-mode atomic force microscopy (3D-MFP AFM, Asylum Research, CA). The AFM measurements were repeated after further annealing at 160 °C to ensure that the structures were equilibrated.

3. Simulation Method for the Multi-Chain Adsorption from Melt. We consider a system of $N = 400$ star-shaped polymers. A star-shaped polymer is represented as a spherical core with f attached arms ($f = 2$, 3, 4, 6, 8, 16, 32) and each arm is composed of $M = 20$ beads.

Table 1. Star-Shaped Polystyrene (PS) Molecular Characteristics

polymer	functionality (f)[a]	M_n^{arm} (kg/mol)[b]	PDI[c]	γ (mJ/m^2)
StarPS-3arm-19K[d]	3	19	1.09	30.5
StarPS-4arm-4K[d]	4	4	1.03	29.1
StarPS-8arm-10K[d]	8	10	1.03	29.3
StarPS-16arm-13K	16	13	1.02	29.1
StarPS-32arm-9K	32	9	1.03	28.9
StarPS-64arm-9K	64	9	1.02	28.5

[a]Functionality, f, determined by the ratio $(M_w)_{star}/(M_n)_{arm}$. [b]From membrane osmometry in toluene at 35 °C. [c]From SEC in THF at 40 °C calibrated with linear PS standards. [d]Purchased from Polmer Source Inc.

We set the diameter of the polymer beads as the unit length, σ; the core radius is $R_c = 0.25\,\sigma$ for star with $f = 4$, 6, 8, and 16 but for $f = 32$ to accommodate a higher number of grafted chains, so $R_c = 1.0\,\sigma$. For linear chains, denoted as a star-shaped polymer with $f = 2$, the core is of the same size as the beads composing the arms. Interactions between polymer beads are described by the cut-and-shifted Lennard-Jones potential with ε and σ as the energy and range parameters, and the cutoff distance $r_c = 2.5\,\sigma$. The beads along a chain are connected with their neighbors via a stiff harmonic spring, $V_H(r) = k(r - l_o)^2$, where $l_o = 0.99\,\sigma$ is the equilibrium length of the spring, and $k = 5000\,\varepsilon/\sigma^2$ is the spring constant. The core−core and core-monomer interactions are modeled as purely repulsive Weeks−Chandler−Andersen[27] with modifications that account for differences between the particle sizes.[28] The energy and interaction range parameter are chosen to be the same for these interactions such that $\varepsilon_{cc} = \varepsilon_{cb} = \varepsilon$ and $\sigma_{cc} = \sigma_{cb} = \sigma$.

Simulations were performed in an $L \times L \times H$ cuboidal box with periodic boundary conditions in all three directions and the minimum-image convention applied. The surface was represented by a stuctureless solid slab with dimensions $L \times L \times l$ and with thickness l no less than the maximum range of interactions between beads. The dimensions of the surface are always large enough for polymers which can assume various conformations to avoid interacting with their own periodic images. The simulation conditions ensure that the polymers are at finite densities within the simulation cell, so there is an equilibrium state where the polymers are adsorbed. In principle, the polymer could be adsorbed no either face of the slab, but they cannot interact with each other because l is larger than the interaction range and H is much larger that in typical polymer dimensions (as measured by the radius of gyrations, R_c). Hence, the two surfaces are essentially isolated from one another. For simulations involving a surface, an effective bead-surface potential was used[29] based on integrating the Lennard-Jones interactions arising from a homogeneous distribution of sites with the surface

$$V(r) = \varepsilon_s\left[\frac{2}{15}\left(\frac{\sigma}{r}\right)^9 - \left(\frac{\sigma}{r}\right)^3\right] \quad (1)$$

where ε_S controls the strength of the bead-surface attraction and r represents here the distance between a bead and a surface. The simulations were performed by the large-scale atomic/molecular massively parallel simulator (LAMMPS) developed as Sandia National Laboratories[30] The mass of particle scales linearly with volume, so that $m_c = R_c^3 m_b$ for the mass of the polymer bead, m_b, and core, m_c, respectively. Simulations were performed in the NVT ensemble after equilibration in the NVP ensemble at the desired temperature. Constant pressure was applied in the xy-directions. Time averaging was conducted for $O(10^8)$ time steps after equilibration. The time step was set to $\delta t = 0.005\tau$, where $\tau = \sigma\,(m_b/\varepsilon)^{1/2}$ is the unit of time. Temperature and pressure are measured in units of ε/k_B and σ^3/ε, respectively. k_B is Boltzmann's constant. All simulations were performed at atmospheric pressure, which closely corresponds in reduced units to $P = 0$.

dx.doi.org/10.1021/ma4024119 | Macromolecules 2014, 47, 1137−1143

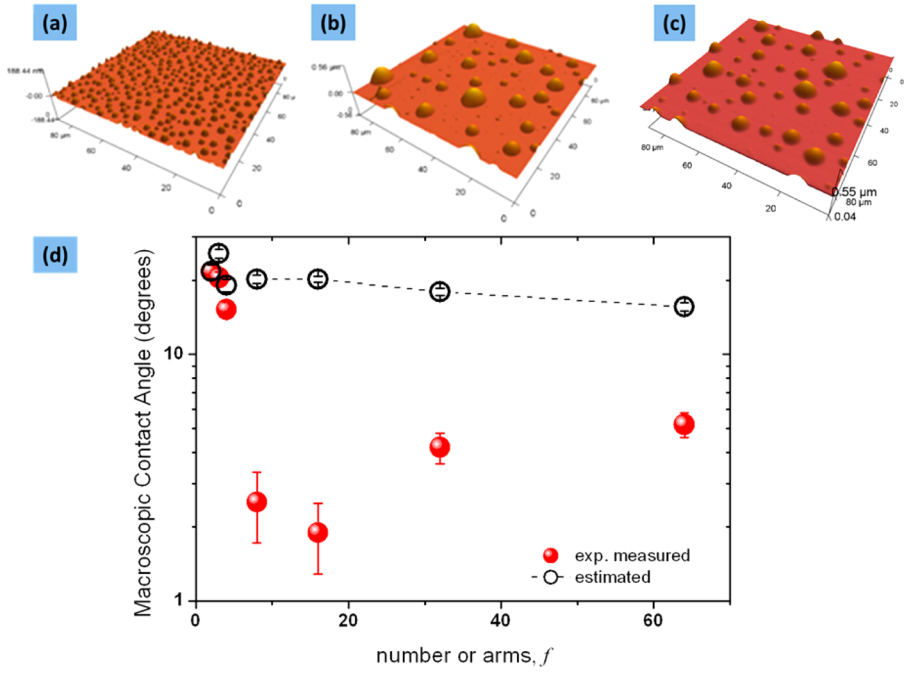

Figure 1. (a–c) 3D AFM images of a 16-, 32-, and 64-arms star-shaped PS films with thickness of approximately 30 nm that were annealed for several days at 160 °C and dewetted are shown in parts a, b, and c, respectively. (d) Experimentally determined macroscopic contact angles, θ_∞, are plotted as a function of f of the star-shaped polymer (red symbols); the open black symbols-dashed lines are the contact angles estimated using Young's equation.

RESULTS AND DISCUSSION

We begin our discussion of the effect of polymer architecture on the wetting of PS molecules on oxidized silicon surfaces by discussing the macroscopic contact angles, θ_∞, of the macroscopic droplets, formed during the final stage of dewetting. For more details on the molecular characteristics of the polymer used in this study see Table 1. Typical AFM images for the star-shaped polymer samples with f = 16, 32, and 64 are shown in Figure 1, parts a, b, and c, respectively. The morphologies for the linear PS, and 3-, 4-, and 8-arms star-shaped PS samples that had dewet are not shown here; they are shown in ref 19. The values of θ_∞ were extracted using the relation $\tan(\theta_\infty/2) = H/R_D$, where H is the height and R_D the radius of the droplet, and are plotted as a function of f in Figure 1d (red solid symbols). Clearly, θ_∞ decreases with increasing functionality for f up to 16; for f = 16, θ_∞ (16-arm) = 1.9 ± 0.6°, which is more than an order of magnitude smaller than the corresponding θ_∞ for linear chain PS (θ_∞(linear) = 21.8 ± 1°). For functionalities larger than $f \sim 16$, θ_∞ increases and appears to reach a plateau near f = 64, where θ_∞ (64-arm) is approximately 2.7 times higher than for f = 16, yet smaller than that of linear chain PS.

The connection between the contact angles and the interfacial energies may be reasonably well described by Young's equation $\gamma \cos \theta_\infty = \gamma_{SV} - \gamma_{SL}$. Young's equation dictates that decreasing values of γ would result in decreasing values of θ_∞. The increased frustrated packing of the star-shaped polymers in the bulk with increasing f is known to be responsible for the decrease of the surface tension of star-shaped molecules with increasing f.[21,22] Therefore, a natural question is whether the dependence of the θ_∞ on the f could be rationalized in terms of changes in their surface tensions. This could be tested by assuming that the difference $\gamma_{SV} - \gamma_{SL}$ is constant and independent of f. If this were true then θ_∞ of each polymer, θ^S_∞, may be estimated using Young's equation, $\cos \theta^s_\infty = (\gamma_L)/(\gamma_S) \cos \theta^L_\infty$.

The surface tensions of the star-shaped molecules were estimated based on the work of Archer and co-workers who used linear response theory to show that the surface tension of star-shaped polymers may be reasonably described by $\gamma^s(M_n) = \gamma^s(\infty) + \rho RT(n_e U^e + U^b)/(M^S_n)$. In this equation $\gamma^s(\infty)$ is the surface tension for infinite number-average molecular weight, ρ is the bulk density, R is the universal gas constant (8.314 J K^{-1} mol^{-1}), T is the temperature, M_n is the number-average molecular weight, and n_e is the number of ends (or f for the case of star-shaped polymers). U^e represents the effective attractive interactions between the interface and the chain ends, and U^b represents repulsive interactions between the interface and the branch points.[21,22] The estimated values of γ at T = 160 °C are listed in Table 1; for the linear PS we used γ^L=30.1 mJ/m^2.[31] θ^S_{eq} as a function of f is plotted as open black symbols (dashed line) in Figure 1d. For low functionalities of f = 3 and 4, the value of θ^S_∞ are comparable with the experimentally measured values (Figure 1d). However, for $f > 4$, θ^S_∞ is significantly larger than the experimentally measured θ_∞ indicating that the observed trends cannot be explained solely from the progressively lower surface tensions of the star-shaped polymers with increasing f. Moreover, the progressively lower surface tensions of the star-shaped polymers with increasing f cannot account for the nonmonotonic relation of θ_∞ with f (Figure 1d). As discussed below, the observed trends stem primarily from the effect of f on the adsorption behavior of the star-shaped molecules on substrates.

One can get additional insights into the nature and strength of interfacial interactions between the polymers and the substrate by considering consequences of the effective interface potential on the system. For the specific situation involving linear chain PS/SiO$_x$/Si system, the effective interface potential may be written as[9,13]

dx.doi.org/10.1021/ma4024119 | Macromolecules 2014, 47, 1137–1143

$$\phi(h) = -\frac{A_{\text{air-PS-SiO}}}{12\pi h^2} - \frac{A_{\text{air-PS-Si}} - A_{\text{air-PS-SiO}}}{12\pi(h + d_{\text{ox}})^2} + \frac{\beta}{h^8} \quad (2)$$

where d_{ox} is the thickness of the SiO_x layer; $A_{\text{air-PS-SiO}}$ and $A_{\text{air-PS-Si}}$ are the Hamaker constants of the air/PS/SiO_x and air/PS/Si systems, respectively ($A_{\text{air-PS-SiOx}} = 2.93 \times 10^{-20}$ J and $A_{\text{air-PS-Si}} = -4.87 \times 10^{-20}$ J). The first two terms in eq 2 are the classical unretarded van der Waals forces between the media PS, SiO_x, Si while the third term, β, represents the strength of the short-range interactions of the polymer with the substrate. The effective interface potential exhibits a minimum, ϕ_{min}, at a thickness h^* which corresponds to the thickness of the adsorbed layer that remains on the SiO_x substrate after dewetting. ϕ_{min} provides information about θ_∞ of the macroscopic droplets through the Young-Dupre equation, $\phi_{min} = \gamma(\cos\theta_\infty - 1)$.[32] β was estimated by adjusting its value until the depth of ϕ_{min} matched that which was estimated from the experimentally measured θ_∞. The global minimum, h_{min}, is connected to the magnitude of β and is plotted as a function of f in Figure 2 (open black symbols). It is evident that

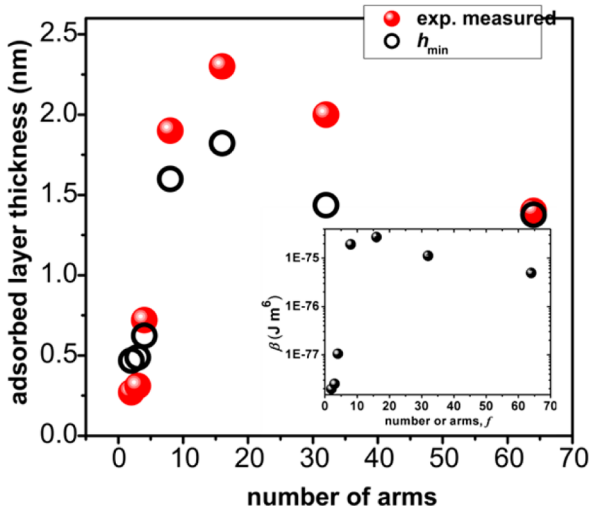

Figure 2. Plot showing the variation of the adsorbed layer thickness as a function of the number of arms of the star-shaped polymers (red solid symbols) and the corresponding thickness based on the global minimum (h_{min}) of the effective interfacial potential ϕ, eq 1 (open black symbols). The inset shows the short-range attraction (β) of the star-shaped polymers with the oxidized silicon wafers as a function of the star-shaped functionality.

h^* increases with increasing f, reaching its highest value when $f \sim 16$, beyond which it decreases for larger f. The values of the strength of the short-range interactions, β, also exhibit a similar trend with f, as shown in the inset of Figure 2; for $f = 16$, β is more than 2 orders of magnitude larger than that of linear chain PS, whereas for $f = 64$, β is nearly 5 times lower than the case of $f = 16$; It however remains 2 orders of magnitude higher than that of linear chain PS.

The dependence of h^* on f manifests the differences between the strength of the entropically driven attraction of star-shaped and linear polymers on the substrate. In principle this behavior provided insight into the *thickness* of the adsorbed layer. As previously shown, for $f \leq 8$ the values of h_{min} were consistent with the experimentally measured adsorbed layer of these systems.[19] For the case of PS linear chain and for the star-shaped polymer with $f = 3$ and $f = 4$, the adsorbed layer "broke up" into nanodroplets; its thickness was estimated by considering the total volume per area (see ref 19). For $f \geq 8$ the initial film thickness remained on the substrate at the final stage of dewetting was initially thicker than h^*, because it was composed of nonadsorbed chains. Hence the values of h^* were determined as follows. Samples were initially immersed in a good solvent (toluene) so that the chains not directly adsorbed onto the substrate would be dissolved. These samples were then placed for several days into an oven at 160 °C under vacuum (i.e., well above the T_g of the samples), during which the adsorbed layer was observed to remain remarkably stable for most samples. The adsorbed layer in each sample was scratched/scored so the substrate to be exposed, then its thickness measured using AFM, Figure 3. Only for the case of the $f = 64$ sample, the adsorbed layer was not uniform and morphological instabilities occurred (Figure 3d); these instabilities, however, did not grow with time so the adsorbed layer did not break up to form nanodroplets. The adsorbed layers for all other samples remained stable, uniform in thickness; their thicknesses are plotted in Figure 2 (solid red symbols). The magnitudes of these film thicknesses and their dependences on f are similar to those of h^* (open black symbols). The sample possessing $f = 16$ arms possessed the thickest adsorbed layer.

To gain further insights on the effect of functionality on the unusual wetting properties and the observed trends in θ_∞, h^*, and β of these molecules, molecular dynamics (MD) simulations were performed. The approach we adopted was to describe both the adsorption and conformational behavior of a single chain and of multichain adsorption from a melt, using a bead−spring model. In general, the adsorption behavior, the conformation of macromolecules close to a substrate, and the thickness of the adsorbed layer is driven by the competition between the gain in enthalpy from binding monomers to the substrate and the conformational entropic cost of the macromolecules as they confine themselves to a thickness smaller than their unperturbed polymers size.[33] Despite the fact that an adsorbed polymer chain gains adsorption energy that is typically much less than kT per monomer (order of conformational entropy), the entire chain, due to the many adsorption contacts, may gain much larger energy than the lost conformational entropy. Hence, a molecule has the tendency to maximize the number of contacts with the substrate, subject to the conformational entropic cost. Details of the simulation procedures we followed for the adsorption behavior of isolated chains are published elsewhere.[34,35] Briefly, Θ-solvent conditions were used for the case of single chain adsorption in order mimic intramolecular interactions similar to those of chains in the melt state.

We begin by discussing the conformational properties of single chains on an adsorbing surface under Θ-solvent conditions. The radius of gyration of a macromolecule in the proximity of the surface is

$$\langle R_g^2 \rangle = \frac{1}{N_b^2} \langle \sum_{i=1}^{N_b} \sum_{j=1}^{N_b} (\vec{r}_i - \vec{r}_j)^2 \rangle \quad (3)$$

where $N_b = Nf + 1$ is the total number of beads in a star-shaped polymer and $\vec{r}_i$ represents the position of bead i. Near the surface it is necessary to consider the dimensions of the star-shaped molecule with respect to the surface. Thus, we resolve the vector $\vec{r}_i - \vec{r}_j$ in eq 2 in the components perpendicular (z) and parallel to the surface (xy) such that $\langle R_g^2 \rangle = \langle R_g^2 \rangle_z + \langle R_g^2 \rangle_{xy}$.

dx.doi.org/10.1021/ma4024119 | Macromolecules 2014, 47, 1137−1143

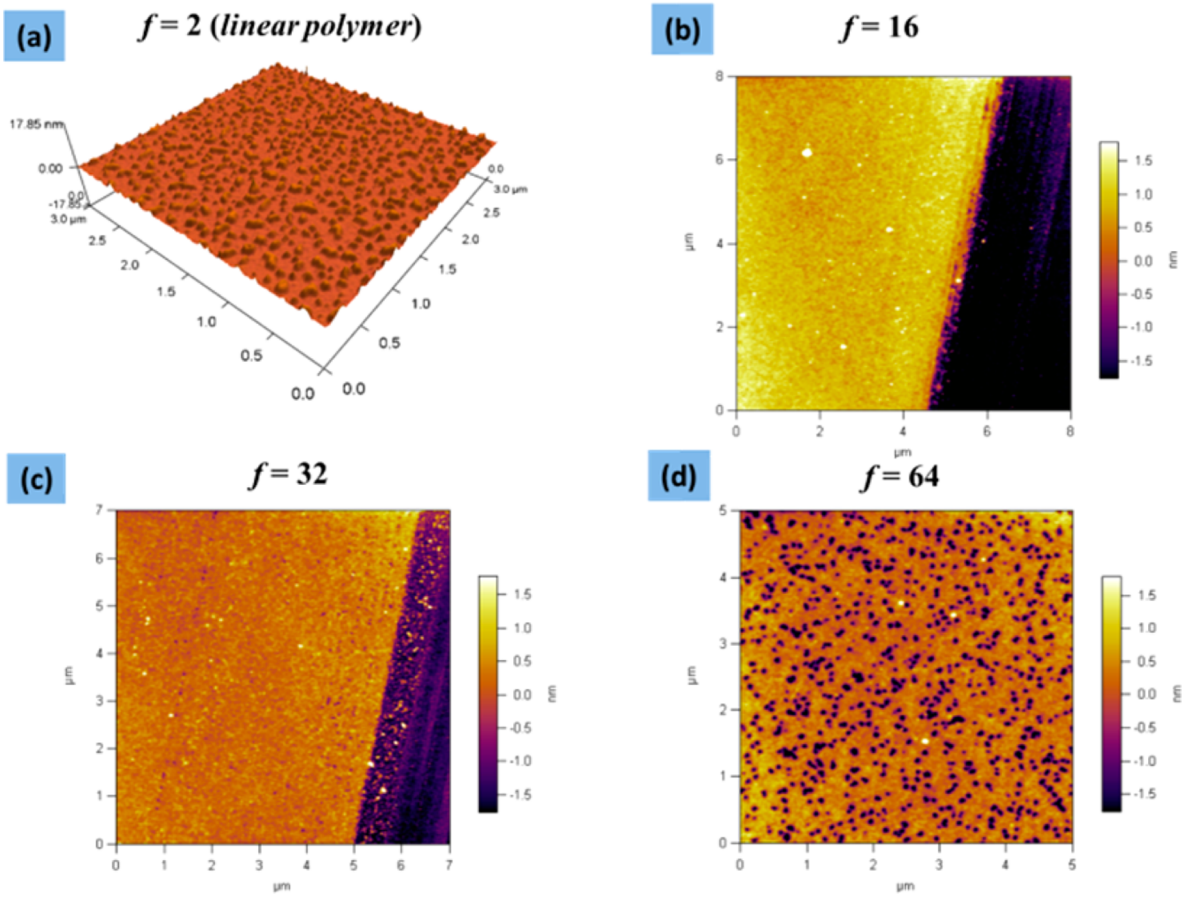

Figure 3. AFM images of the structures of the adsorbed layers after annealing of 2 days at 160 °C for (a) the linear chain PS ($f = 2$), (b) star-shaped PS with $f = 16$, (c) star-shaped PS with $f = 32$, and (d) star-shaped PS with $f = 64$. For the star-shaped polymer samples with $f = 16$ and 32, the samples were scored after immersing the samples in a good solvent bath and prior to annealing.

The ratio of the perpendicular and parallel components, $\langle R_g^2\rangle_z/\langle R_g^2\rangle_{xy}$, was estimated for the case of singly adsorbed chains for Θ-solvent conditions and is shown as a function of f in Figure 4a (open red symbols). It is clear that the ratio $\langle R_g^2\rangle_z/\langle R_g^2\rangle_{xy}$ monotonically increases with f. This could be understood in terms of the decreasing softness of the star-shaped polymers with increasing f,[36,37] and as a result, it gradually decreases its ability to deform upon adsorption on the surface in order to maximize contacts with the surface. It is important to emphasize that our simulations also reveal that the number of the adsorbed monomers increases with increasing f indicating an enhanced chain adsorption/affinity to the substrate with increasing f.

Intermolecular interactions can significantly affect the structure of the adsorbed molecules in melt conditions. The ratio $\langle R_g^2\rangle_z/\langle R_g^2\rangle_{xy}$ of the adsorbed molecules from the melt (multichain adsorption) is plotted in Figure 4a (black solid symbols). It is interesting to note that the ratio $\langle R_g^2\rangle_z/\langle R_g^2\rangle_{xy}$ of an adsorbed molecule from the melt is significantly larger than that of an isolated adsorbed molecule, indicating that each molecule adsorbed from the melt occupies less surface area. The dependence of $\langle R_g^2\rangle_z/\langle R_g^2\rangle_{xy}$ on f is such that it achieves a maximum for $f = 8$. For $f > 8$, the ratio $\langle R_g^2\rangle_z/\langle R_g^2\rangle_{xy}$ decreases. The number of adsorbed molecules per simulation unit area, ρ_{ads}, is plotted as a function of f in Figure 4b (solid black symbols). ρ_{ads} was also estimated from the experiments by considering the thickness of the adsorbed layer, the density of the PS, and the molecular mass (open blue symbols, Figure 4b). There is a very good agreement between the experiments and the simulations. ρ_{ads} increases with f, as the effective entopic attraction of the molecules to the substrate increases, reaching a maximum value for $f = 8$ and then decreases with further increase of f. The decease of ρ_{ads} for $f > 8$ indicates a gradually reduced ability of the star-shaped polymers to "crowd" and adsorb onto the surface. The decreasing density of the molecules on the surface is accompanied by a corresponding decrease of $\langle R_g^2\rangle_z/\langle R_g^2\rangle_{xy}$. This is because the molecules attempt to maximize the available area; note that with increasing f the ratio $\langle R_g^2\rangle_z/\langle R_g^2\rangle_{xy}$ in the melt remains larger that the case of a single adsorbed chain.

Simulations and theory reveal that due to their topology and related entropic effects, the chain segments close to the star-polymer core are more stretched due to enhanced interchain interactions. This creates a gradient in the monomer density, increasing from the vicinity of the core to the chain ends; the effect increases with f.[36−40] The high concentration of monomers close to the center of the star-shaped polymers results in an effective long-range (compared to the monomer size) entropic repulsion between molecules as they become closer, and the entropic repulsion becomes gradually more long-ranged with increasing f.[36,37] Recently, Egorov et al., showed that for adsorbed star shaped polymers in good solvent conditions, stronger repulsive interactions existed near the surface, compared interactions far from the surface.[41] Clearly, the strength of the entropic repulsion increases with increasing f. We anticipate that an enhanced entropic repulsion between

dx.doi.org/10.1021/ma4024119 | Macromolecules 2014, 47, 1137−1143

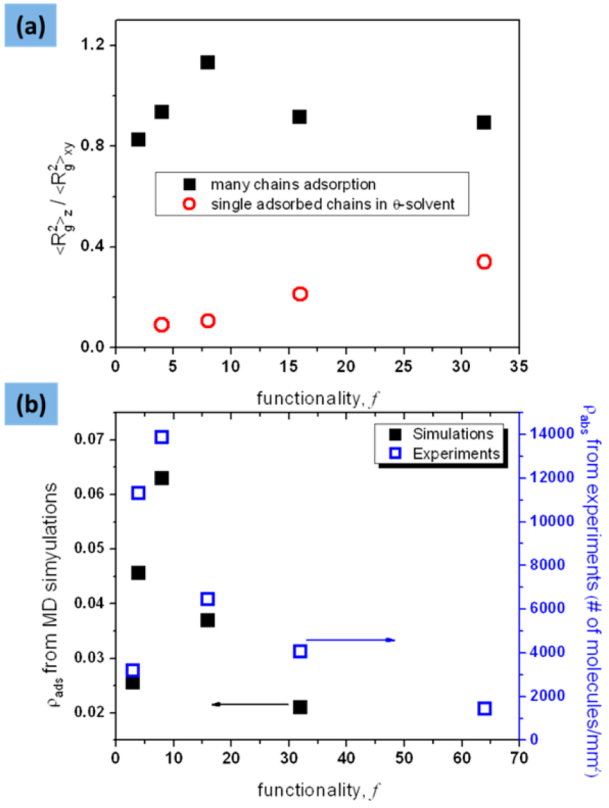

Figure 4. (a) Ratio of the parallel and perpendicular components of the mean squared radii of gyration of the adsorbed chains as a function of functionality f, for stars that are singly adsorbed (open red symbols), are adsorbed from a melt, or show multichain adsorption (solid black symbols). (b) Plots showing the variation of the density of the adsorbed macromolecules, ρ_{ads}, from the MD simulations (solid black symbols, left scale), and from experiments (open blue symbols, right scale).

adsorbed stars relative to stars in the bulk would also exist in the melt state. Our data indicate that by increasing f there is a competition between the increasing adsorption of star-shaped polymers to the surface (associated with a gradually decreasing entropic penalty upon adsorption) and the increasing entropic repulsion of the adsorbed chains that reduce the ability of more molecules to reside at the surface. The intermolecular entropic repulsion balances and eventually suppresses the effective entropic attraction of the polymer with the surface. These competing entopic effects control the wetting/dewetting behavior of the star-shaped polymers, giving rise to a minimum in θ_∞ and a maximum of h_{min} as a function of f.

CONCLUSIONS

In summary, we showed that by simply varying the functionality of star-shaped polymers, the wetting properties could be dramatically altered, or tailored, in a controllable fashion. Our experiments and simulations showed that the wetting characteristics of the star-shaped PS on oxidized silicon wafers are determined by the competition between interfacially attractive conformational entropic effects and intermolecular entropic repulsions. The interplay of these effects can be readily controlled through changes of the star-shaped functionality. Because of its entropic origin, varying the functionality provides an essential tool for controlling the wetting behavior of polymers on substrates. Applications in a range of industries that utilize polymer thin films, from adhesion and coatings for magnetic storage to various microelectronic applications, would benefit from the outcome of our experiments.

AUTHOR INFORMATION

Corresponding Author

*(P.F.G.) E-mail: pfgreen@umich.edu.

Notes

The authors declare no competing financial interest.

ACKNOWLEDGMENTS

This work was supported by the National Science Foundation (NSF), Division of Materials Research (DMR-1305749).

REFERENCES

(1) Bonn, D.; Eggers, J.; Indekeu, J.; Meunier, J.; Rolley, E. *Rev. Mod. Phys.* **2009**, *81* (2), 739−805.
(2) de Gennes, P. G.; Brochard-Wyart, F.; Quere, D., *Capillarity and Wetting Phenomena*. Springer-Verlag New York, Inc.: New York, 2004.
(3) Degennes, P. G. *Rev. Mod. Phys.* **1985**, *57* (3), 827−863.
(4) Leger, L.; Joanny, J. F. *Rep. Prog. Phys.* **1992**, *55* (4), 431−486.
(5) Young, T. *Philos. Trans. R. Soc. London* **1805**, *95*, 65−87.
(6) Sharma, A. *Langmuir* **1993**, *9* (3), 861−869.
(7) Vanoss, C. J.; Chaudhury, M. K.; Good, R. J. *Chem. Rev.* **1988**, *88* (6), 927−941.
(8) Israelachvili, J. N. *Intermolecular and Surface Forces*. 3rd ed.; Academic Press: Burlington, MA, 2011.
(9) Seemann, R.; Herminghaus, S.; Jacobs, K. *Phys. Rev. Lett.* **2001**, *86* (24), 5534−5537.
(10) Reiter, G. *Phys. Rev. Lett.* **1992**, *68* (1), 75−78.
(11) Yerushalmirozen, R.; Klein, J. *Langmuir* **1995**, *11* (7), 2806−2814.
(12) Reiter, G. *Langmuir* **1993**, *9* (5), 1344−1351.
(13) Green, P. F.; Ganesan, V. *Eur. Phys. J. E* **2003**, *12* (3), 449−454.
(14) Muller-Buschbaum, P.; Vanhoorne, P.; Scheumann, V.; Stamm, M. *Europhys. Lett.* **1997**, *40* (6), 655−660.
(15) Muller, M.; MacDowell, L. G.; Muller-Buschbaum, P.; Wunnike, O.; Stamm, M. *J. Chem. Phys.* **2001**, *115* (21), 9960−9969.
(16) Yerushalmirozen, R.; Klein, J.; Fetters, L. J. *Science* **1994**, *263* (5148), 793−795.
(17) Mansky, P.; Liu, Y.; Huang, E.; Russell, T. P.; Hawker, C. J. *Science* **1997**, *275* (5305), 1458−1460.
(18) Xu, L.; Yu, X.; Shi, T.; An, L. *Macromolecules* **2008**, *41* (1), 21−24.
(19) Glynos, E.; Frieberg, B.; Green, P. F. *Phys. Rev. Lett.* **2011**, *107* (11), 5.
(20) Striolo, A.; Prausnitz, J. M. *J. Chem. Phys.* **2001**, *114* (19), 8565−8572.
(21) Minnikanti, V. S.; Archer, L. A. *Macromolecules* **2006**, *39* (22), 7718−7728.
(22) Qian, Z. Y.; Minnikanti, V. S.; Sauer, B. B.; Dee, G. T.; Archer, L. A. *Macromolecules* **2008**, *41* (13), 5007−5013.
(23) Kosmas, M. K. *Macromolecules* **1990**, *23* (7), 2061−2065.
(24) Hadjichristidis, N.; Iatrou, H.; Pispas, S.; Pitsikalis, M. *J. Polym. Sci., Part A: Polym. Chem.* **2000**, *38* (18), 3211−3234.
(25) Uhrig, D.; Mays, J. W. *J. Polym. Sci., Part A: Polym. Chem.* **2005**, *43* (24), 6179−6222.
(26) Roovers, J.; Zhou, L. L.; Toporowski, P. M.; Vanderzwan, M.; Iatrou, H.; Hadjichristidis, N. *Macromolecules* **1993**, *26* (16), 4324−4331.
(27) Weeks, J. D.; Chandler, D.; Andersen, H. C. *J. Chem. Phys.* **1971**, *54* (12), 5237−+.
(28) Sewell, T. D.; Menikoff, R.; Bedrov, D.; Smith, G. D. *J. Chem. Phys.* **2003**, *119* (14), 7417−7426.
(29) Sides, S. W.; Grest, G. S.; Stevens, M. J. K. *Macromolecules* **2002**, *35* (2), 566−573.
(30) Plimpton, S. J. *J. Comput. Phys.* **1995**, *117*, 1.

(31) Dee, G. T.; Sauer, B. B. *J. Colloid Interface Sci.* **1992**, *152* (1), 85−103.
(32) Sharma, A. *Langmuir* **1998**, *14* (17), 4915−4928.
(33) Rubinstein, M.; Colby, R. H., *Polymer Physics*; Oxford University Press: New York, 2003.
(34) Chremos, A.; Camp, P. J.; Glynos, E.; Koutsos, V. *Soft Matter* **2010**, *6* (7), 1483−1493.
(35) Chremos, A.; Glynos, E.; Koutsos, V.; Camp, P. J. *Soft Matter* **2009**, *5* (3), 637−645.
(36) Likos, C. N.; Lowen, H.; Watzlawek, M.; Abbas, B.; Jucknischke, O.; Allgaier, J.; Richter, D. *Phys. Rev. Lett.* **1998**, *80* (20), 4450−4453.
(37) Likos, C. N. *Phys. Rep.—Rev. Sect. Phys. Lett.* **2001**, *348* (4−5), 267−439.
(38) Pakula, T. *Comput. Theor. Polym. Sci.* **1998**, *8* (1−2), 21−30.
(39) Daoud, M.; Cotton, J. P. *J. Phys.* **1982**, *43* (3), 531−538.
(40) Vlassopoulos, D.; Fytas, G.; Pakula, T.; Roovers, J. *J. Phys.: Condens. Matter* **2001**, *13* (41), R855−R876.
(41) Egorov, S. A.; Paturej, J.; Likos, C. N.; Milchev, A. *Macromolecules* **2013**, *46* (9), 3648−3653.